

Driven-dissipative fermionized topological phases of strongly interacting bosons

Arkajyoti Maity,^{1,*} Bimalendu Deb,² and Jan-Michael Rost¹

¹*Max Planck Institut fur Physik komplexer Systeme,
Nöthnitzer Str. 38, Dresden, 01187, Germany*

²*Indian Association for the Cultivation of Science,
2a and 2b Raja S.C. Mallik Road, Jadavpur, Kolkata 700032, West Bengal, India*

(Dated: October 23, 2024)

We study the optical response of a one-dimensional array of strongly nonlinear optical microcavities with alternating tunnel transmissivities, mimicking the paradigmatic Su-Schrieffer Heeger model. We show that the non-equilibrium steady state of the bosonic system contains clear signatures of fermionization when the intra-cavity Kerr non-linearity is stronger than both losses and inter-site tunnel coupling. Furthermore, changing the experimentally controllable parameters detuning and driving strength, in a topologically non-trivial phase, one can selectively excite either the bulk or edge modes or both modes, revealing interesting topological properties in a non-equilibrium system.

The physics of symmetry-protected topological phases (SPT) has been a topic of intense research over the last decade [1–3]. Topologically non-trivial phases of matter were initially predicted and classified for non-interacting systems [4], with the appearance of robust edge states serving as the primary experimental evidence. First observed [5, 6] in insulating materials, topological physics has since been realized with artificial designer lattices in mechanical [7, 8], ultracold atomic [9, 10], photonic [11, 12] and polaritonic [13, 14] settings, unraveling novel SPTs, edge states involving synthetic dimensions [12], quasi-crystalline order [15, 16] and much more. Interestingly and contrary to initial expectations, studies with moderate interactions between particles have led to several novel classifications of SPTs [17, 18]. In photonic platforms, nonlinear interactions have led to topological phase transitions [19, 20], mode-mixing [21, 22], topo-

logically non-trivial gap-solitons [23–26] and the emission of symmetry-protected coherent light [27, 28]. These studies, however, were performed for weak interactions, where mean field theories are applicable. In the strong interaction regime, more robust SPTs may arise. Examples are the observation of edge states in the many-body Su-Schrieffer-Heeger model, emulated with Rydberg atoms [29] or the emergence of topological order [30], such as the fractional quantum Hall phase [31, 32], recently realised, with artificial gauge fields in photonic setups [33, 34]. Photonic platforms also enable controlled engineering of gain and losses leading to the recent development of non-Hermitian topological phases [35–43]. Applications include perfectly directional robust topological amplification and frequency conversion [40, 44]. Topological photonics in such non-equilibrium open systems, coupled additionally with strong non-linearities is a nascent but promising field of research [45–48].

Here, we identify topological signatures in a non-equilibrium state of strongly correlated bosons and demonstrate how they can be manipulated by changing experimentally accessible parameters. The state is created in a strongly interacting Su-Schrieffer-Heeger (SSH) lattice [49] of optical micro-cavities mutually coupled by tunnelling and driven by a coherent laser field. We specifically focus on the strongly nonlinear regime, where non-trivial quantum correlations between bosons, constrained in one spatial dimension, herald the onset of a Tonks-Girardeau gas [50–52] of ‘fermionized bosons’. Variants of the SSH model, including particle-particle interactions, driving and losses have been explored over the years leading to several theoretical proposals [53–56] and experimental realisations [23, 27, 28, 57]. However, to the best of our knowledge, the interplay between strong correlation-induced fermionization and topology in an interacting non-equilibrium SSH system has not been studied. Indeed, we observe that the reduced spatial dimensions of interacting bosons, in conjunction with drive and dissipation can produce highly non-trivial ‘fermionized’ steady states, where one can selectively excite edge modes, bulk modes or both by changing the driving parameters, without having to resort to any predefined

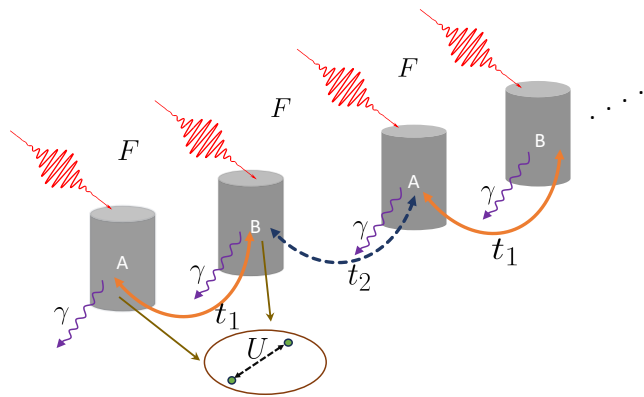


FIG. 1. Schematic diagram of our proposed set-up, featuring an array of non-linear semiconductor microcavities with alternating inter-pillar spacings for mimicking an SSH model. The cavities are driven homogeneously by an external laser field F .

* maity@pks.mpg.de

state preparation. To be specific, we consider a coupled one-dimensional array of M optical cavities embedded in a non-linear semiconductor medium [58, 59], with each cavity being subjected to uniform driving, as sketched in Fig. 1. Cavity polaritons, which are composite bosons originating from the strong coupling between semiconductor quantum well excitons and cavity photons are particularly well suited for our proposal and have already shown great promise in emulating interacting non-Hermitian topological lattice models [14, 23, 60–63]. Their excitonic component can give rise to a sizeable Kerr nonlinearity [64–67], while their photonic component allows for engineering loss and gain in the system. In our model, we restrict the physical description to a single mode of frequency ω_0 per cavity by ensuring that the energy spacing between neighbouring modes of a single cavity is much larger than all other energy scales. The Hamiltonian describes an SSH Bose-Hubbard model, where the Hubbard interaction term U arises due to the Kerr non-linearity [65] of the intra-cavity medium. Alternating couplings (t_1 and t_2) are created by engineering staggered overlap between nearest neighbour cavity modes [14, 23]. Driving every cavity uniformly with coherent monochromatic light of amplitude F and frequency ω_p , we recast the Hamiltonian in a frame rotating with the drive [64] as $H_{\text{tot}} = H_{\text{sys}} + H_{\text{drive}}$, where

$$H_{\text{sys}} = \hbar\Delta\omega \sum_j (a_j^\dagger a_j + b_j^\dagger b_j) - t_1 \sum_j (a_j^\dagger b_j + h.c.) - t_2 \sum_j (b_j^\dagger a_{j+1} + h.c.) + U \sum_j (a_j^\dagger a_j^\dagger a_j a_j + b_j^\dagger b_j^\dagger b_j b_j) \quad (1)$$

with the detuning $\Delta\omega = \omega_0 - \omega_p$ of the cavity frequency from the pump frequency. The one-photon resonant drive is described by

$$H_{\text{drive}} = \sum_j F(a_j^\dagger + b_j^\dagger) + h.c., \quad (2)$$

where $a_j(b_j)$ denotes bosonic annihilation operators for sublattice A (B) in unit cell j , as is the case in the SSH model (see Fig. 1).

To compute the steady state, under particle loss from the system at a dissipation rate γ , we assume Born-Markov conditions and make use of the Lindblad master equation [68],

$$\partial\rho/\partial t = -i[H, \rho] + D[\rho] \quad (3)$$

with

$$D[\rho] = \frac{\gamma}{2} \sum_j (2a_j \rho a_j^\dagger - a_j^\dagger a_j \rho - \rho a_j^\dagger a_j) + \frac{\gamma}{2} \sum_j (2b_j \rho b_j^\dagger - b_j^\dagger b_j \rho - \rho b_j^\dagger b_j). \quad (4)$$

Since in most experimentally realizable setups, the propagation of the pump light through the sample is

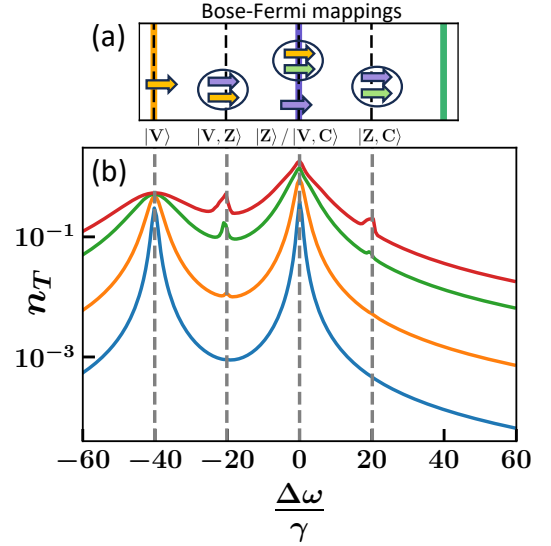


FIG. 2. (b) Transmission spectrum of $M = 4$ cavities in the impenetrable boson limit, with $t_1/\gamma=2, t_2/\gamma=40$ in Eq. (1) computed from the steady state $\partial\rho/\partial t = 0$ in Eq. (3). The different curves correspond from below to increasing pump amplitudes $F/\gamma = 0.1, 1.0, 3.0, 5.0$. The vertical dashed lines indicate the detunings for the spectral peaks, derived analytically from the eigenvalues of the Fermi-mapping. Each mapping is sketched in (a) with colored arrows representing the different orbital contributions, either from the bulk (orange ($|V\rangle$)) and green ($|C\rangle$)), or the topological edge (light purple, $|Z\rangle$). All two-particle mappings are circled.

inhibited [69, 70], properties of the system are inferred from the spectrum and coherence of the transmitted light. The total transmitted intensity is proportional to the average total number of particles, $n_T = \langle \sum_j (a_j^\dagger a_j + b_j^\dagger b_j) \rangle$, in the steady state [23], while the near-field transmission [23, 71] corresponds to the site resolved population.

For better understanding, we briefly line out the most important features of the eigenstates of any one-dimensional system of \mathbf{N} impenetrable bosons ($U \rightarrow \infty$) in the absence of pumping and dissipation. A more detailed analysis is given in Appendix A. The extreme correlation-induced fermionization of bosons implies that strongly interacting bosons can be mapped to a non-interacting fermionic system. The spatial eigenfunction, $\psi_B(\mathbf{x})$ of \mathbf{N} bosons at positions $\mathbf{x} = (x_1, \dots, x_N)^\dagger$ can be mapped to a fermionic one $\psi_F(\mathbf{x})$, as $\psi_B(\mathbf{x}) = |\psi_F(\mathbf{x})|$. The fermionic wavefunction can then be classified by the occupation numbers of single-particle orbitals [50]. One can invoke the coordinate Bethe ansatz [72, 73] to write $\psi_B(\mathbf{x})$ as

$$\psi_B(\mathbf{x}) \sim \det[\Phi_j(x_l)] \prod_{1 \leq j < l \leq N} \text{sgn}(x_j - x_l). \quad (5)$$

The number of permitted single-particle orbitals $\Phi_j(x_l)$, depend on the degrees of freedom of the system and the

sign function is multiplied with the Slater determinant to fix the particle statistics from fermionic to bosonic. The total energy E_N of the state is then exactly replicated by the sum of the energies $\epsilon(j_i)$ of the filled single-particle orbitals,

$$E_N = \sum_{i=1}^N \epsilon(j_i), \quad (6)$$

where j_i denotes the orbital occupied by the i 'th mapped particle. Subjecting such a bosonic system to external driving and dissipation, especially in lattice environments can create very non-trivial Bose-Fermi mappings in the steady state as demonstrated for the case of a simple 1D chain [74]. We focus on investigating the interplay of fermionization and topology in the driven-dissipative SSH Bose-Hubbard model described by (1) for both periodic and open boundary conditions. Although imposing periodic boundary conditions leads to interesting features of quasi-momentum quantized mapping and non-trivial band couplings, we leave its discussions to Appendix B and focus here on the open boundary case, where topological effects appear physically in the form of edge states via the bulk-boundary correspondence [75]. We numer-

for a range of drive amplitudes F . The Bloch state quasi-momenta q (defined in Appendix B) are no longer good quantum numbers for open boundary conditions. Hence, the single particle orbital energies (ξ) are obtained by exact diagonalization of (1) with $U = 0$. Fixing the value of γ at unity, the resonant detuning at which the pump can excite any allowed N -boson excited state is now expected at $\Delta\omega = E_{\text{total}}/N = \sum_{i=1}^N \xi_i/N$. Fig. 2 illustrates how our numerically determined mean particle number n_T exhibits peaks at the analytical Bose-to-Fermi mapped states. For small F , the pump excites an $N = 1$ bosonic state giving rise to single mapped fermionic states, namely $|V\rangle$ from the bulk at detuning $\Delta\omega \approx -40$ and $|Z\rangle$ from the topological edge at $\Delta\omega = 0$, while for increasing field strength F , $N > 1$ bosonic states are created through multi-photon processes, giving rise to additional two fermion peaks (indicated with circles in the sketch of mapped states Fig. 2a) appearing near $\Delta\omega = \pm 20$.

The zero detuning case is fascinating because it can realize two different mappings. The first mapping $|Z\rangle$, already mentioned, corresponds to many-body bosonic states represented by zero-energy single-particle states which are the degenerate topological gapless edge modes. The second mapping corresponds to a $N = 2$ excited state $|V, C\rangle$, with one mapped fermion in $|V\rangle$ and the other in its chiral partner, the upper energy state, $|C\rangle$, such that their energies sum up to zero. Note, that the mapping $|C\rangle$ by itself cannot be excited with a single photon due to symmetry constraints [76].

Unlike $|Z\rangle$, the two-particle state $|V, C\rangle$ is completely immersed in the lattice bulk. The results of Fig. 2 suggest that the population of edge versus bulk states changes with increasing drive strength F differently, for the fermionized resonances which would allow the selective population of bulk and edge modes. This is indeed the case, as shown in Fig. 3(a). When pumping at zero detuning with small F , exclusively edge states are populated (black line), while pumping at detuning $\Delta\omega$, corresponding to the fermionized resonance $|V\rangle$ (blue line), only bulk modes are excited. Not surprisingly, the fraction of edge states of the double excitation $|V, Z\rangle$ (red line) comprised of a bulk and an edge state, is hardly sensitive to the drive strength. Suppose one is interested in switching between edge and bulk excitation. This can be achieved at zero detuning by simply increasing F , since small F will favour the singly excited edge state $|Z\rangle$, while larger F will also populate the doubly excited bulk state $|V, C\rangle$, (see black line).

To gain further insight into the microscopic nature of the many-body states, we investigate the intensity correlations in the near-field transmission. It is well known that although the density distributions are identical, the one-dimensional hard core bosonic wavefunction is not the same as the non-interacting fermionic case. This can be verified by calculations of the momentum distribution in periodic boundary conditions or by probing any odd-order correlation function. For example, the momentum

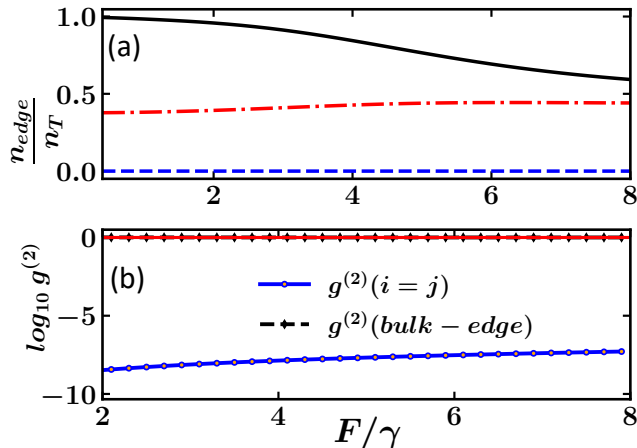


FIG. 3. The edge-population fraction, plotted against the drive amplitude F is shown in (a), with the cavity-pump detuning ($\Delta\omega/\gamma$) locked in at three distinct analytically predicted fermionized resonances: $|V\rangle$ (blue dashed), $|V, Z\rangle$ (red dash-dotted) and $\Delta\omega/\gamma = 0$ (black solid), corresponding to either $|Z\rangle$ or $|V, C\rangle$ (b) Plot of the lattice averaged zero time auto ($i = j$) and bulk-edge intensity cross-correlations against F/γ for $\Delta\omega = 0$ in the driving regime where both bulk and edge are populated. The orange solid line is indicative of non-correlated Poissonian photon emission statistics.

ically evaluate the steady state density matrix from (3) for $M = 4$ cavities in the topologically non-trivial open boundary configuration $U \rightarrow \infty$ and $t_1 < t_2$ respecting the Born-Markov regime of weak system-reservoir coupling ($\gamma \ll t_2 \ll U \rightarrow \infty$) by choosing $t_1/\gamma = 2$ and $t_2/\gamma = 40$. The expected transmission (obtained from n_T) is shown in Fig. 2, as a function of the cavity-pump detuning ($\Delta\omega$)

distribution of a Tonks gas is very different to that of free fermions. [51, 77, 78]. Any even-order correlation should however be identical because it depends on field densities [79–81].

Having already established that our system's steady state can host both topological fermionized edge state(s) and bulk states at zero detuning, we investigate how the bosonic modes on the bulk and edge are correlated to each other. To do so, we calculate the equal time second-order cross-correlation function between lattice sites i and j , defined as

$$g^{(2)}(i, j) = \frac{\langle c_i^\dagger c_j^\dagger c_j c_i \rangle}{\langle c_i^\dagger c_i \rangle \langle c_j^\dagger c_j \rangle}, \quad (7)$$

where c_j is the boson annihilation of site j , belonging to sublattice A(B) depending on whether j is odd(even) and the expectation value is calculated at steady state. Fig. 3(b) shows the lattice averaged on-site and bulk-edge correlations for the topological configuration at zero detuning $\Delta\omega=0$. One can observe that the on-site ($i=j$) correlations are extremely small, indicating strong anti-bunching in the transmission statistics. This is to be expected since the repulsive interaction effectively fermionizes the system, such that a single site cannot host more than one particle: the mapping to fermions implies Pauli blocking of two similar fermions at the same spatial coordinate. This is analogous to strong non-linearity induced photon blockade [74, 82], used to generate single photons. Interestingly, the bulk-edge correlations of the transmission are fully separable, being coherent for a large range of drive parameters. This can be explained by analysing the drive-controlled excitation, as the inherent fermionization governs the intensity correlations. For drive amplitudes F , where the steady state can host fermionized bulk modes $|V, C\rangle$, the correlation between the edge $|Z\rangle$ and the bulk gets suppressed due to the topological protection of the edge states imposed by chiral symmetry [83]. This means that each cavity can act as a single photon source, tunable from emitting solely from the edges to emitting from the bulk and the edge by increasing the driving strength at zero detuning. However, since the emission statistics are uncorrelated, any perturbation in the bulk will not disturb the emission from the edges, as long as the symmetries protecting the phase [83, 84] are maintained. We conclude our discussion on these fermionized topological phases by assessing for which parameter regime one can observe fermionization experimentally. A crucial question for experiments is the effective interaction strength U/T , $T = \max(t_1, t_2)$ (the largest kinetic energy scales in the system) at which the bosonic system behaves as its fermionized counterpart. To this end, we analyze the excitation dynamics as a function of U/T for fixed driving strength $F/\gamma=1$. Fig. 4(a) shows the total transmission n_T versus the detuning $\Delta\omega/\gamma$. The spectrum shows a strong peak at $\Delta\omega_{1p}$, corresponding to the one-boson excitation and a second peak of the two-boson excitation, whose position $\Delta\omega_{2p}$ gets increasingly blue shifted from $\Delta\omega_{1p}$ for

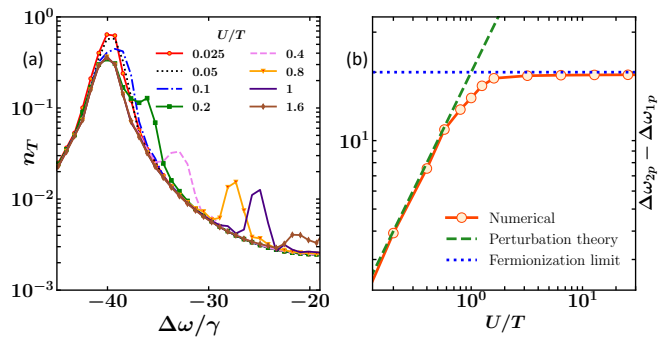


FIG. 4. The lowest energy one boson and two boson peaks in the transmission spectrum as calculated from the steady state are shown in (a) for a range of interaction strengths U/T . Panel (b) shows the shift in resonant detunings for the two peaks against the interaction strength. For $U/T \approx 2$, the shift saturates to the predicted shifts of the fermionized mapped states (blue dotted line). The green dashed line shows the linear variation of the shifts against U/T , as predicted by perturbation theory.

larger U/T . Eventually, $\Delta\omega_{2p}$ reaches an asymptotic value (seen in Fig. 4(b)), where the two-boson excitation coincides in the steady state with the 'fermionized' 2-particle peak $|V, Z\rangle$, which is roughly the case at $U/T \approx 2$. The behaviour can be understood using perturbation theory. In the $U=0$ limit, a two-particle bosonic state will have both particles occupying ψ_V , the wavefunction of the lowest energy single body orbital $|V\rangle$. The zeroth order wavefunction can be written as $\psi_0 = \psi_V \otimes \psi_V$. The resonant detunings at $U=0$, given by (6), for the one-particle ($\Delta\omega_{1p}$) and two-particle ($\Delta\omega_{2p}$) states coincide since the energy of the one-boson state is just twice the energy of the two-boson state. Increasing U , the energy gets shifted perturbatively by $\Delta E_0 = U \langle \psi_0 | \hat{\alpha} | \psi_0 \rangle$ with $\hat{\alpha} = \sum_i (a_i^\dagger a_i^\dagger a_i a_i + b_i^\dagger b_i^\dagger b_i b_i)$. Since the two-particle ground state wavefunction ψ_0 , for our system, is a spatially symmetric superposition of the bulk sites, we have $\Delta E_0 \approx U$. Fig. 4(b) reveals a linear increase of the shift $\Delta\omega_{2p} - \Delta\omega_{1p}$ in the interaction regime of perturbatively small U/T , eventually crossing over to the fermionization regime at large U/T .

In conclusion, we have provided a scenario where the steady state of a many-body system can be steered from bulk to edge modes by just changing the strength of the optical drive. This has been enabled by the interplay of topology and strong correlation-induced fermionization of bosons. As a consequence, we could show how to control the transmission intensity and statistics from the bulk and edge modes without resorting to prior state preparation. Finally and importantly, we have demonstrated that the predicted phenomena occur at parameters which can be realized in state-of-the-art photonic/polaritonic platforms [14, 23, 63, 85]

Acknowledgements: A.M would like to thank Kingshuk Adhikary and Panos Giannakeas for helpful discussions. The authors would also like to acknowledge the open-

source package QuTiP [86], used in some numerical calculations.

Appendix A: Bose-Fermi mapping in a 1D hard-core continuum Bose gas

The natural starting point for a Bose-Fermi mapping of an impenetrable one-dimensional gas of bosons with contact interaction $U \rightarrow \infty$ is the coordinate Bethe ansatz (5). In equilibrium, this gas, known as the Lieb-Liniger model [73], is a rare, fully integrable system. To evaluate the eigenstates with periodic boundary conditions one first inserts plane waves into the Bethe ansatz, $\Phi_j(x_l) = e^{ik_j x_l}$; a rigorous treatment can be found in Refs. [72, 73]. For $U \rightarrow \infty$, known as the Tonks-Girardeau limit, the eigen solutions for N bosons get fermionized. The wavefunction for bosons at positions $\mathbf{x} = (x_1, \dots, x_N)^\dagger$, χ_N is given by

$$\chi_N(\mathbf{x}) = \frac{C}{\sqrt{N!}} \det [e^{ik_j x_l}] \prod_{1 \leq l < j \leq N} \text{sgn}(x_j - x_l) \quad (\text{A1})$$

with the quasi-momentum k_j for the j 'th boson and normalization constant C . The construction ensures that $\chi_N(\mathbf{x})$ vanishes for $x_j = x_l$. Furthermore, the total momentum of the eigenstate is given by $P_N = \sum_j k_j$ and the total energy by $E_N = \sum_j k_j^2/2$ ($\hbar = 1$). Note, however, that the quasi momenta do not represent the true momentum of the bosons, although their sums are necessarily equal [87]. Ensuring periodic boundary conditions by confining our system on a ring of length L , the wavefunctions (A1) must necessarily satisfy $\chi_N(\mathbf{x})|_{x_i=0} = \chi_N(\mathbf{x})|_{x_i=L}$ for all $i=1, \dots, N$. With (A1) it is easy to see that this requires quantising the quasimomenta,

$$\begin{aligned} k_i &= (n_i + 1/2) 2\pi/L & N = \text{even}, \\ k_i &= n_i 2\pi/L & N = \text{odd}, \end{aligned} \quad (\text{A2})$$

where n_i is an integer. This peculiar quantization of quasimomenta is one of the hallmarks of fermionization.

Appendix B: Spectral signatures of fermionization in periodic boundary conditions

Having established in brief some salient points on the fermionization of the 1D hard-core Bose gas, we move on to tackling the driven dissipative hard-core SSH Bose-Hubbard model described in Eqns. (1) and (2) with periodic boundary conditions imposed. Since the SSH model hosts a periodic lattice potential, for periodic boundary conditions, in the non-driven regime, any fermionized N particle bosonic state can be classified via the Bloch states of the Hamiltonian, $|q_1^{m_1}, q_2^{m_2}, \dots, q_N^{m_N}\rangle$, where m_i denotes the band index and q_i denotes the crystal quasi-momentum of the mapping for the i 'th boson. An important point to note is that for a purely non-interacting

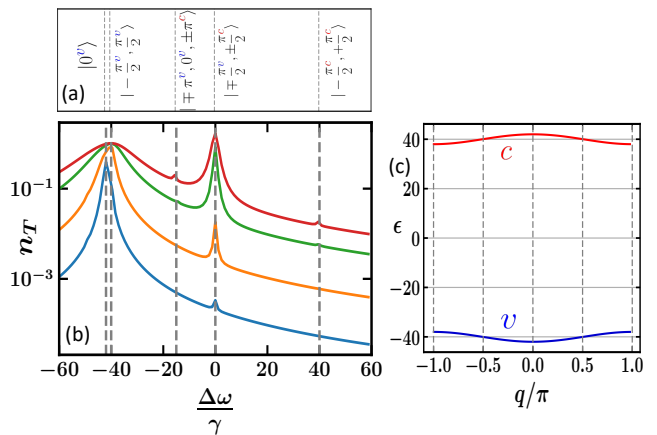


FIG. 5. (b) Transmission spectrum of a closed chain of $M=4$ cavities and $t_1/\gamma=2, t_2/\gamma=40$ in (1) computed from the steady state, for $F/\gamma = 0.1$ (blue), 1.0 (orange), 3.0 (green), 5.0 (red). (a) The detunings, corresponding to the fermionized resonances are indicated by dashed lines with each mapping being explicitly written out in terms of the quasimomenta and band contributions. (c) The band diagram of the SSH Hamiltonian for our chosen parameters is shown as a reference to the mappings depicted in (a).

bosonic system, there is no restriction in two or more particles occupying the same orbital (q_i, m_i), while in the strongly correlated regime, fermionic states defined by the mapping (5) are Pauli blocked from having identical quantum numbers. Energy E and total momentum P of the bosonic state are given by $E = \sum_i \epsilon(m_i, q_i)$ and $P = \sum_i q_i$, respectively, although the momentum distributions do not map [50, 87]. When the drive is turned on, it can create non-trivial steady states, by generating excitations from the vacuum state to any allowed N boson 'fermionized' state.

We observe this in Fig. 5, where we plot the total transmitted intensity, numerically evaluated with (3) in the limit of impenetrable bosons and weak dissipation ($\gamma \ll \max(t_1, t_2) \ll U \rightarrow \infty$) for a range of drive strengths. We choose the lattice spacing between unit cells to be unity and the other parameters chosen are the same as those used in the main text. Fig.5(b) reveals resonances of the transmitted spectrum at specific detunings $\Delta\omega$. The position of these resonances does not depend on the driving strength, but their height sensitively depends on F . The positions are determined by the frequencies, at which the pump can excite any N particle fermionized many-body bosonic eigenstate $|q_1^{m_1}, q_2^{m_2}, \dots, q_N^{m_N}\rangle$ in the non equilibrium steady state and those frequencies analytically given by the total energy of the single particle orbitals normalised to the total number of particles,

$$\Delta\omega = E_{\text{total}}/N = \sum_{i=1}^N \epsilon_{m_i}(q_i)/N. \quad (\text{B1})$$

For small driving $F \ll \gamma$, the pump induces a steady state which has the largest overlap with the vacuum state

and a single bosonic excitation $N = 1$, which is Fermi-mapped to $|0^v\rangle$, a fermion in the lower Bloch band, denoted by v , at quasimomentum zero. For larger values of the drive amplitude, higher Fock states are excited (since the system has no $U(1)$ symmetry), with the constraint $\sum_i q_i = 0 \pmod{2\pi}$, due to momentum conservation and the quantization condition for the quasimomenta, see (A2) and [74]. Interestingly, in a two-band model like the SSH, the pump can also excite many-body bosonic states which map to fermionic excitations in two bands of the SSH model (v and c), subject to the momentum

conservation and the energy resonance relation (B1). We find very good agreement of the numerically evaluated peak positions with that predicted by (B1) and list all the single-band and coupled-band mappings in Fig. 5(a). The band diagram for the SSH model in our chosen parameters is provided in Fig. 5(c) for reference. It should be noted that the transmission spectra upon exchanging t_1 and t_2 are identical. This is expected from their identical Bose-Fermi mappings due to the same equilibrium band structure. However, they are topologically not equivalent, and the implications of this fact are presented in the main text.

-
- [1] M. Z. Hasan and C. L. Kane, Colloquium: topological insulators, *Rev. Mod. Phys.* **82**, 3045 (2010).
- [2] X.-L. Qi and S.-C. Zhang, Topological insulators and superconductors, *Rev. Mod. Phys.* **83**, 1057 (2011).
- [3] T. Senthil, Symmetry-protected topological phases of quantum matter, *Annu. Rev. Condens. Matter Phys.* **6**, 299 (2015).
- [4] C.-K. Chiu, J. C. Y. Teo, A. P. Schnyder, and S. Ryu, Classification of topological quantum matter with symmetries, *Rev. Mod. Phys.* **88**, 035005 (2016).
- [5] Y. Xu, I. Miotkowski, C. Liu, J. Tian, H. Nam, N. Alidoust, J. Hu, C.-K. Shih, M. Z. Hasan, and Y. P. Chen, Observation of topological surface state quantum hall effect in an intrinsic three-dimensional topological insulator, *Nature Physics* **10**, 956 (2014).
- [6] D. Hsieh, Y. Xia, D. Qian, L. Wray, J. Dil, F. Meier, J. Osterwalder, L. Patthey, J. Checkelsky, N. P. Ong, *et al.*, A tunable topological insulator in the spin helical dirac transport regime, *Nature* **460**, 1101 (2009).
- [7] S. D. Huber, Topological mechanics, *Nature Physics* **12**, 621 (2016).
- [8] G. Ma, M. Xiao, and C. T. Chan, Topological phases in acoustic and mechanical systems, *Nature Reviews Physics* **1**, 281 (2019).
- [9] N. Cooper, J. Dalibard, and I. Spielman, Topological bands for ultracold atoms, *Rev. Mod. Phys.* **91**, 015005 (2019).
- [10] N. Goldman, J. C. Budich, and P. Zoller, Topological quantum matter with ultracold gases in optical lattices, *Nature Physics* **12**, 639 (2016).
- [11] L. Lu, J. D. Joannopoulos, and M. Soljačić, Topological photonics, *Nature photonics* **8**, 821 (2014).
- [12] T. Ozawa and H. M. Price, Topological quantum matter in synthetic dimensions, *Nature Reviews Physics* **1**, 349 (2019).
- [13] S. Klembt, T. Harder, O. Egorov, K. Winkler, R. Ge, M. Bandres, M. Emmerling, L. Worschech, T. Liew, M. Segev, *et al.*, Exciton-polariton topological insulator, *Nature* **562**, 552 (2018).
- [14] D. D. Solnyshkov, G. Malpuech, P. St-Jean, S. Ravets, J. Bloch, and A. Amo, Microcavity polaritons for topological photonics, *Optical Materials Express* **11**, 1119 (2021).
- [15] Y. E. Kraus, Y. Lahini, Z. Ringel, M. Verbin, and O. Zilberberg, Topological states and adiabatic pumping in quasicrystals, *Physical Review Letters* **109**, 106402 (2012).
- [16] A. Maity and A. Chakrabarti, Engineering insulator-metal transition in a class of decorated aperiodic lattices: A quantum dynamical study, *Physics Letters A* **406**, 127452 (2021).
- [17] C. Wang, A. C. Potter, and T. Senthil, Classification of interacting electronic topological insulators in three dimensions, *Science* **343**, 629 (2014).
- [18] S. Rachel, Interacting topological insulators: a review, *Reports on Progress in Physics* **81**, 116501 (2018).
- [19] L. J. Maczewsky, M. Heinrich, M. Kremer, S. K. Ivanov, M. Ehrhardt, F. Martinez, Y. V. Kartashov, V. V. Konotop, L. Torner, D. Bauer, *et al.*, Nonlinearity-induced photonic topological insulator, *Science* **370**, 701 (2020).
- [20] Y. Hadad, J. C. Soric, A. B. Khanikaev, and A. Alu, Self-induced topological protection in nonlinear circuit arrays, *Nature Electronics* **1**, 178 (2018).
- [21] S. Mittal, E. A. Goldschmidt, and M. Hafezi, A topological source of quantum light, *Nature* **561**, 502 (2018).
- [22] S. Kruk, A. Poddubny, D. Smirnova, L. Wang, A. Slobozhanyuk, A. Shorokhov, I. Kravchenko, B. Luther-Davies, and Y. Kivshar, Nonlinear light generation in topological nanostructures, *Nature nanotechnology* **14**, 126 (2019).
- [23] N. Pernet, P. St-Jean, D. D. Solnyshkov, G. Malpuech, N. Carlon Zambon, Q. Fontaine, B. Real, O. Jamadi, A. Lemaitre, M. Morassi, *et al.*, Gap solitons in a one-dimensional driven-dissipative topological lattice, *Nature Physics* **18**, 678 (2022).
- [24] S. Mukherjee and M. C. Rechtsman, Observation of floquet solitons in a topological bandgap, *Science* **368**, 856 (2020).
- [25] D. Solnyshkov, O. Bleu, B. Teklu, and G. Malpuech, Chirality of topological gap solitons in bosonic dimer chains, *Physical Review Letters* **118**, 023901 (2017).
- [26] M. Guo, S. Xia, N. Wang, D. Song, Z. Chen, and J. Yang, Weakly nonlinear topological gap solitons in su-schrieffer-heeger photonic lattices, *Optics Letters* **45**, 6466 (2020).
- [27] P. St-Jean, V. Goblot, E. Galopin, A. Lemaitre, T. Ozawa, L. Le Gratiet, I. Sagnes, J. Bloch, and A. Amo, Lasing in topological edge states of a one-dimensional lattice, *Nature Photonics* **11**, 651 (2017).
- [28] M. Parto, S. Wittek, H. Hodaei, G. Harari, M. A. Bandres, J. Ren, M. C. Rechtsman, M. Segev, D. N. Christodoulides, and M. Khajavikhan, Edge-mode lasing

- in 1d topological active arrays, *Physical Review Letters* **120**, 113901 (2018).
- [29] S. De Léséleuc, V. Lienhard, P. Scholl, D. Barredo, S. Weber, N. Lang, H. P. Büchler, T. Lahaye, and A. Browaeys, Observation of a symmetry-protected topological phase of interacting bosons with rydberg atoms, *Science* **365**, 775 (2019).
- [30] X.-G. Wen, Colloquium: Zoo of quantum-topological phases of matter, *Rev. Mod. Phys.* **89**, 041004 (2017).
- [31] J. Jain, Theory of the fractional quantum hall effect, *Physical Review B* **41**, 7653 (1990).
- [32] H. L. Stormer, D. C. Tsui, and A. C. Gossard, The fractional quantum hall effect, *Rev. Mod. Phys.* **71**, S298 (1999).
- [33] C. Wang, F.-M. Liu, M.-C. Chen, H. Chen, X.-H. Zhao, C. Ying, Z.-X. Shang, J.-W. Wang, Y.-H. Huo, C.-Z. Peng, *et al.*, Realization of fractional quantum hall state with interacting photons, *Science* **384**, 579 (2024).
- [34] P. Knüppel, S. Ravets, M. Kroner, S. Fält, W. Wegscheider, and A. Imamoglu, Nonlinear optics in the fractional quantum hall regime, *Nature* **572**, 91 (2019).
- [35] Z. Gong, Y. Ashida, K. Kawabata, K. Takasan, S. Higashikawa, and M. Ueda, Topological phases of non-hermitian systems, *Phys. Rev. X* **8**, 031079 (2018).
- [36] E. J. Bergholtz, J. C. Budich, and F. K. Kunst, Exceptional topology of non-hermitian systems, *Rev. Mod. Phys.* **93**, 015005 (2021).
- [37] A. McDonald, R. Hanai, and A. A. Clerk, Nonequilibrium stationary states of quantum non-hermitian lattice models, *Phys. Rev. B* **105**, 064302 (2022).
- [38] S. Yao and Z. Wang, Edge states and topological invariants of non-hermitian systems, *Phys. Rev. Lett.* **121**, 086803 (2018).
- [39] D. S. Borgnia, A. J. Kruchkov, and R.-J. Slager, Non-hermitian boundary modes and topology, *Phys. Rev. Lett.* **124**, 056802 (2020).
- [40] C. C. Wanjura, M. Brunelli, and A. Nunnenkamp, Topological framework for directional amplification in driven-dissipative cavity arrays, *Nature communications* **11**, 3149 (2020).
- [41] Á. Gómez-León, T. Ramos, A. González-Tudela, and D. Porras, Driven-dissipative topological phases in parametric resonator arrays, *Quantum* **7**, 1016 (2023).
- [42] V. P. Flynn, E. Cobanera, and L. Viola, Topology by dissipation: Majorana bosons in metastable quadratic markovian dynamics, *Phys. Rev. Lett.* **127**, 245701 (2021).
- [43] F. Song, S. Yao, and Z. Wang, Non-hermitian skin effect and chiral damping in open quantum systems, *Phys. Rev. Lett.* **123**, 170401 (2019).
- [44] L.-X. Guo, L.-L. Wan, L.-G. Si, and Y. Wu, Topological amplification and frequency conversion in a photonic lattice with a two-photon driving, *Phys. Rev. A* **108**, 013512 (2023).
- [45] W. N. Faugno and T. Ozawa, Interaction-induced non-hermitian topological phases from a dynamical gauge field, *Phys. Rev. Lett.* **129**, 180401 (2022).
- [46] F. Roccati, M. Bello, Z. Gong, M. Ueda, F. Ciccarello, A. Chenu, and A. Carollo, Hermitian and non-hermitian topology from photon-mediated interactions, *Nature Communications* **15**, 2400 (2024).
- [47] K. Cao and S.-P. Kou, Topological phases of many-body non-hermitian systems, *Physical Review B* **109**, 155434 (2024).
- [48] K. Kawabata, K. Shiozaki, and S. Ryu, Many-body topology of non-hermitian systems, *Physical Review B* **105**, 165137 (2022).
- [49] A. J. Heeger, S. Kivelson, J. R. Schrieffer, and W. P. Su, Solitons in conducting polymers, *Rev. Mod. Phys.* **60**, 781 (1988).
- [50] M. Girardeau, Relationship between systems of impenetrable bosons and fermions in one dimension, *Journal of Mathematical Physics* **1**, 516 (1960).
- [51] B. Paredes, A. Widera, V. Murg, O. Mandel, S. Fölling, I. Cirac, G. V. Shlyapnikov, T. W. Hänsch, and I. Bloch, Tonks-girardeau gas of ultracold atoms in an optical lattice, *Nature* **429**, 277 (2004).
- [52] T. Kinoshita, T. Wenger, and D. S. Weiss, Observation of a one-dimensional tonks-girardeau gas, *Science* **305**, 1125 (2004).
- [53] P. M. Azcona and C. Downing, Doublons, topology and interactions in a one-dimensional lattice, *Scientific reports* **11**, 12540 (2021).
- [54] P. Matveeva, D. Gutman, and S. T. Carr, Weakly interacting one-dimensional topological insulators: A bosonization approach, *Physical Review B* **109**, 165436 (2024).
- [55] W. N. Faugno and T. Ozawa, Interaction-induced non-hermitian topological phases from a dynamical gauge field, *Phys. Rev. Lett.* **129**, 180401 (2022).
- [56] A. A. Stepanenko and M. A. Gorlach, Interaction-induced topological states of photon pairs, *Physical Review A* **102**, 013510 (2020).
- [57] C. Downing, T. Sturges, G. Weick, M. Stobińska, and L. Martín-Moreno, Topological phases of polaritons in a cavity waveguide, *Physical Review Letters* **123**, 217401 (2019).
- [58] G. Khitrova, H. Gibbs, F. Jahnke, M. Kira, and S. W. Koch, Nonlinear optics of normal-mode-coupling semiconductor microcavities, *Rev. Mod. Phys.* **71**, 1591 (1999).
- [59] B. Deveaud, *The physics of semiconductor microcavities*, (2007).
- [60] X. Xu, R. Bao, and T. C. Liew, Non-hermitian topological exciton-polariton corner modes, *Physical Review B* **106**, L201302 (2022).
- [61] A. Szameit and M. C. Rechtsman, Discrete nonlinear topological photonics, *Nature Physics* , 1 (2024).
- [62] S. Mandal, R. Banerjee, E. A. Ostrovskaya, and T. C. H. Liew, Nonreciprocal transport of exciton polaritons in a non-hermitian chain, *Physical Review Letters* **125**, 123902 (2020).
- [63] D. Zhao, Z. Wang, L. Yang, Y. Zhong, X. Xi, Z. Zhu, M. Gong, Q. Tu, Y. Meng, B. Yan, *et al.*, Observation of tunable topological polaritons in a cavity waveguide, *arXiv preprint arXiv:2401.10450* (2024).
- [64] I. Carusotto and C. Ciuti, Quantum fluids of light, *Rev. Mod. Phys.* **85**, 299 (2013).
- [65] D. E. Chang, V. Vuletić, and M. D. Lukin, Quantum nonlinear optics—photon by photon, *Nature Photonics* **8**, 685 (2014).
- [66] A. Kavokin and G. Malpuech, *Cavity polaritons* (Elsevier, 2003).
- [67] T. M. Autry, G. Nardin, C. L. Smallwood, K. Silverman, D. Bajoni, A. Lemaître, S. Bouchoule, J. Bloch, and S. Cundiff, Excitation ladder of cavity polaritons, *Phys. Rev. Lett.* **125**, 067403 (2020).

- [68] H.-P. Breuer and F. Petruccione, *The theory of open quantum systems* (Oxford University Press, USA, 2002).
- [69] O. El Daïf, A. Baas, T. Guillet, J.-P. Brantut, R. I. Kaitouni, J.-L. Staehli, F. Morier-Genoud, and B. Deveaud, Polariton quantum boxes in semiconductor microcavities, *Applied Physics Letters* **88** (2006).
- [70] A. Amo, S. Pigeon, C. Adrados, J. Lefrere, C. Ciuti, I. Carusotto, R. Houdré, A. Bramati, and E. Giacobino, Quantum fluid properties of polaritons in semiconductor microcavities, *Journal of Modern Optics* **57**, 1900 (2010).
- [71] N. Louvion, D. Gérard, J. Mouette, F. de Fornel, C. Seassal, X. Letartre, A. Rahmani, and S. Callard, Local observation and spectroscopy of optical modes in an active photonic-crystal microcavity, *Phys. Rev. Lett.* **94**, 113907 (2005).
- [72] E. H. Lieb and W. Liniger, Exact analysis of an interacting bose gas. i. the general solution and the ground state, *Physical Review* **130**, 1605 (1963).
- [73] E. H. Lieb, Exact analysis of an interacting bose gas. ii. the excitation spectrum, *Physical Review* **130**, 1616 (1963).
- [74] I. Carusotto, D. Gerace, H. E. Tureci, S. De Liberato, C. Ciuti, and A. Imamoglu, Fermionized photons in an array of driven dissipative nonlinear cavities, *Phys. Rev. Lett.* **103**, 033601 (2009).
- [75] B.-H. Chen and D.-W. Chiou, An elementary rigorous proof of bulk-boundary correspondence in the generalized su-schrieffer-heeger model, *Physics Letters A* **384**, 126168 (2020).
- [76] The mapping $|C\rangle$ is the chiral partner of $|V\rangle$ in the sublattice degrees of freedom (A/B); i.e the relative phase between the amplitudes of the wavefunction on sublattices A and B for both mappings differ by a factor of π . Hence, the mapping will be necessarily absent for $M = 4$, if the one-photon drive excites $|V\rangle$. More formally, we do not observe any signal as $\langle C|H_{\text{drive}}|0\rangle = 0$, where $|0\rangle$ is the many-body vacuum state.
- [77] R. Pezer and H. Buljan, Momentum distribution dynamics of a tonks-girardeau gas: Bragg reflections of a quantum many-body wave packet, *Phys. Rev. Lett.* **98**, 240403 (2007).
- [78] S. Scopa, P. Ruggiero, P. Calabrese, and J. Dubail, One-particle density matrix and momentum distribution of the out-of-equilibrium one-dimensional tonks-girardeau gas: Analytical results at large n , *Phys. Rev. A* **108**, 013324 (2023).
- [79] G. Astrakharchik, J. Boronat, J. Casulleras, and S. Giorgini, Beyond the tonks-girardeau gas: Strongly correlated regime in quasi-one-dimensional bose gases, *Physical Review Letters* **95**, 190407 (2005).
- [80] Y. Hao, Y. Zhang, Y. Liu, and L. Wang, n-body correlation of tonks-girardeau gas, *The European Physical Journal D* **76**, 237 (2022).
- [81] M. Girardeau and E. Wright, Quantum mechanics of one-dimensional trapped tonks gases, arXiv preprint cond-mat/0104585 (2001).
- [82] K. M. Birnbaum, A. Boca, R. Miller, A. D. Boozer, T. E. Northup, and H. J. Kimble, Photon blockade in an optical cavity with one trapped atom, *Nature* **436**, 87 (2005).
- [83] J. K. Asbóth, L. Oroszlány, and A. Pályi, A short course on topological insulators, *Lecture notes in physics* **919** (2016).
- [84] Z. Wang, X. Wang, Z. Hu, D. Bongiovanni, D. Jukić, L. Tang, D. Song, R. Morandotti, Z. Chen, and H. Buljan, Sub-symmetry-protected topological states, *Nature physics* **19**, 992 (2023).
- [85] J. Bloch, I. Carusotto, and M. Wouters, Non-equilibrium bose-einstein condensation in photonic systems, *Nature Reviews Physics* **4**, 470 (2022).
- [86] J. R. Johansson, P. D. Nation, and F. Nori, Qutip: An open-source python framework for the dynamics of open quantum systems, *Computer physics communications* **183**, 1760 (2012).
- [87] V. Yukalov and M. Girardeau, Fermi-bose mapping for one-dimensional bose gases, *Laser Physics Letters* **2**, 375 (2005).